



HAL
open science

Critical behavior and large magnetocaloric effect in $\text{La}_{0.8}\text{K}_{0.175}\text{Li}_{0.025}\text{MnO}_3$ nanopowder manganite

Y. Regaieg, W. Cheikhrouhou-Koubaa, L. Sicard, E.K. Hlil

► **To cite this version:**

Y. Regaieg, W. Cheikhrouhou-Koubaa, L. Sicard, E.K. Hlil. Critical behavior and large magnetocaloric effect in $\text{La}_{0.8}\text{K}_{0.175}\text{Li}_{0.025}\text{MnO}_3$ nanopowder manganite. The European Physical Journal B: Condensed Matter and Complex Systems, 2024, 97 (12), pp.204. 10.1140/epjb/s10051-024-00846-6. hal-04914091

HAL Id: hal-04914091

<https://hal.science/hal-04914091v1>


Submitted on 27 Jan 2025

HAL is a multi-disciplinary open access archive for the deposit and dissemination of scientific research documents, whether they are published or not. The documents may come from teaching and research institutions in France or abroad, or from public or private research centers.

L'archive ouverte pluridisciplinaire **HAL**, est destinée au dépôt et à la diffusion de documents scientifiques de niveau recherche, publiés ou non, émanant des établissements d'enseignement et de recherche français ou étrangers, des laboratoires publics ou privés.



Critical behavior and large magnetocaloric effect in $\text{La}_{0.8}\text{K}_{0.175}\text{Li}_{0.025}\text{MnO}_3$ nanopowder manganite

Y. Regaieg^{1,2,a} , W. Cheikhrouhou-Koubaa¹, L. Sicard³, and E. K. Hlil⁴

¹ LT2S Lab, Digital Research Center of Sfax, Sfax Technoparc, 3021 Sfax, Tunisia

² Faculty of Sciences of Gafsa, University of Gafsa, 2112 Gafsa, Tunisia

³ ITODYS, Université Paris Diderot, UMR 7086 CNRS, 75205 Paris Cedex 13, France

⁴ Univ. Grenoble Alpes, CNRS, Grenoble INP, Institut Néel, 38000 Grenoble, France

Received 18 September 2024 / Accepted 11 December 2024 / Published online 21 December 2024
© The Author(s), under exclusive licence to EDP Sciences, SIF and Springer-Verlag GmbH Germany, part of Springer Nature 2024

Abstract. The rhombohedral $\text{La}_{0.8}\text{K}_{0.175}\text{Li}_{0.025}\text{MnO}_3$ sample was elaborated using the sol-gel method at low temperature of 900 °C. The prepared sample exhibits a second-order paramagnetic-ferromagnetic transition with decreasing temperature. Based on the data of the magnetic measurements, the critical behavior analysis is investigated through various techniques such as modified Arrott plot, Kouvel-Fisher method and critical isotherm analysis. The critical exponents determined using the Kouvel-Fisher method are found to be $\beta = 0.533$ and $\gamma = 1.114$ at $T_C \sim 270$ K. The critical exponent values obtained are in agreement with the values predicted by the mean field model, indicating the existence of long-range magnetic interaction in our synthesized sample. The maximum of the magnetic entropy change is about $3.51 \text{ J kg}^{-1} \text{ K}^{-1}$ under a magnetic applied field change of 5 T. The relative cooling power is found to be 320.5 J kg^{-1} at 5 T. This value represents about 78% of that of standard gadolinium.

1 Introduction

Magnetic refrigeration technology has attracted global interest due to its high energy efficient and environmentally friendly over conventional vapor compression refrigeration technology [1]. The magnetic refrigeration is based on the magnetocaloric effect (MCE) which is an intrinsic property of magnetic materials. The MCE is defined as the thermal heating or cooling response in adiabatic condition of magnetic solids in applying or removing of external magnetic field [2]. In other words, the magnetic entropy change (ΔS_M) or the adiabatic temperature change (ΔT_{ad}) induced by applied magnetic field externally is considered as MCE [3, 4]. Generally, the perovskite manganites, which have the chemical formula $\text{Ln}_{1-x}\text{A}_x\text{MnO}_3$ (Ln: trivalent rare-earth ion and A: monovalent alkali-metal or divalent alkaline-earth ion) showed a wide variety of structural, microstructure, magnetic and electronic properties depending on the nature and concentration of the ions. This family of materials presents a large MCE make promising candidate materials for magnetic refrigeration [5–13]. If not, perovskite manganites are also interesting since they have low cost, high chemical stability, easy elaboration, grain growth to a desired size and the ability to adjust their magnetic transition temperatures by carrier-substitution in

their perovskite Ln or Mn-site [14–17]. In addition, the large MCE could be attributed to the development of the double exchange interaction [18] between Mn^{3+} and Mn^{4+} cations and the strong spin-lattice coupling [19, 20]. Moreover, it has been also demonstrated that the MCE are associated with the complex nature of magnetic phase transition which can be parameterized by critical exponents governing the transitions near the paramagnetic-ferromagnetic region [21]. In fact, the second-order phase transitions around the critical temperature can be described by using the critical exponents [22, 23]. The analysis of critical behavior around the Curie temperature, T_C , would determine the three critical exponents (β , γ and δ) different from those obtained by theoretical models of the mean field model, tricritical mean field model, 3D-Ising model, and 3D-Heisenberg model [24–27]. The mean field model characterizes long-range ferromagnetic interactions, excluding spin correlations near T_C . In the tricritical mean field model, the compound's composition should be close to its tricritical point in the corresponding phase diagram. The 3D-Ising model is associated with short-range interactions between spins. Finally, the 3D-Heisenberg model describes short-range exchange interactions with the presence of localized spin fluctuations around T_C . Besides, the critical behavior of perovskite manganites has been studied by using the Arrott plot (M^2 vs. $\mu_0 H/M$) and the Kouvel-Fisher method derived from isothermal magnetization

^a e-mail: yassine.regaieg@yahoo.fr (corresponding author)

measurements. In principle, the critical behavior near paramagnetic-ferromagnetic phase transition using different techniques has yielded a wide range of values for the critical exponent β [24, 28]. The values range from 0.3 to 0.5: it is 0.5 for the mean field model, 0.365 for 3D-Heisenberg model, 0.325 for the 3D-Ising model [29] and 0.25 for the tricritical mean field model [26]. Furthermore, the critical exponents γ and δ will also given by the reciprocal magnetic susceptibility and the critical isothermal magnetization, respectively.

In previous work [30], we have studied the magnetic and magnetocaloric properties in $\text{La}_{0.8}\text{K}_{0.2-x}\text{Li}_x\text{MnO}_3$ manganites. Indeed, the effect of lithium partial substitution on the critical phenomena in $\text{La}_{1-x}\text{K}_x\text{MnO}_3$ system has not been reported in the literature. In this paper and as a continuing effort, we propose to extend our previous investigation by the study of critical behavior in $\text{La}_{0.8}\text{K}_{0.175}\text{Li}_{0.025}\text{MnO}_3$ perovskite. We present an estimate of the critical exponents near paramagnetic-ferromagnetic phase transition temperature by different techniques such as modified Arrott plot, Kouvel-Fisher method and the critical isotherm analysis. We used the scaling hypothesis to scale the magnetic entropy change to a single universal curve for $\text{La}_{0.8}\text{K}_{0.175}\text{Li}_{0.025}\text{MnO}_3$ nanopowder.

2 Experimental

2.1 Sample synthesis

$\text{La}_{0.8}\text{K}_{0.175}\text{Li}_{0.025}\text{MnO}_3$ nanopowder manganite was prepared by sol-gel method at low temperature [30] by dissolving the stoichiometric amount of precursors La_2O_3 (Suvchem; 99.9%), K_2CO_3 (Alfa Aesar; 99%), Li_2CO_3 (Merck; 99%) and MnO_2 (Sigma Aldrich; 99.99%) with high purity in nitric acid. Citric acid and ethylene glycol were added to guarantee the homogeneity and transparency of the solution. The latter was evaporated at 130 °C until the formation of a gel-like of high viscosity. The temperature was subsequently raised slowly in the air up to 300 °C. After crushing, the powder was heated at 450 °C for 6 h to decompose the organics. The resulting powder was calcined at 650 °C for 12 h and then at 800 °C for the same time period with intermediate grinding. Finally, the sample was pressed as a pellet under a pressure of 4 tonnes and sintered at 900 °C for 24 h.

2.2 Characterization

X-ray diffraction (XRD) patterns were recorded at room temperature in the 2θ range 15–100° with a step size of 0.01° using a Panalytical diffractometer (Empyrean model) equipped with a copper X-ray radiation ($\lambda_{\text{K}\alpha} = 1.5418 \text{ \AA}$). The structure was analyzed by the Rietveld technique [31] using FullProf software [32]. The average crystallite (D_{XRD}) size was calculated from the XRD peak width using the Scherrer

relation [33]. The morphology and size of the grains were obtained by Scanning Electron Microscopy (SEM) using a *Supra40* ZEISS FEG-SEM microscope. Magnetization measurements versus temperature and magnetic applied field were performed employing a MPMS-XL Quantum Design SQUID magnetometer. The crystal structure refinement and temperature-dependence magnetization for our compound have been reported elsewhere [30].

The scaling hypothesis [34] for the second order magnetic phase transition near the T_C is characterized by the critical behavior, which was studied using a set of critical exponents β , γ and δ , associated with a spontaneous magnetization (M_S), a reciprocal magnetic susceptibility (χ_0^{-1}) and a critical isotherm (CI), respectively. These critical exponents are determined using magnetization measurements via the following relations:

$$M_S(T, 0) = \lim(M) = M_0(-\varepsilon)^\beta, \quad \varepsilon < 0, T < T_C \quad (1)$$

$$\chi_0^{-1}(T, 0) = \lim(H/M) = (h_0/M_0)\varepsilon^\gamma, \quad \varepsilon > 0, T > T_C \quad (2)$$

$$M = D(\mu_0 H)^{1/\delta}, \quad \varepsilon = 0, T = T_C, \quad (3)$$

where $\varepsilon = (T - T_C)/T_C$ is the reduced temperature and M_0 , h_0/M_0 , and D are the critical amplitudes.

The validity of the deduced critical exponents in the critical region for ferromagnetic materials was checked by the magnetic equation of state using the scaling hypothesis to form universal scaling curves:

$$M(\mu_0 H, \varepsilon) = \varepsilon^\beta f_\pm(\mu_0 H/\varepsilon^{\beta+\gamma}) \quad (4)$$

where f_+ for $T > T_C$ and f_- for $T < T_C$ are regular analytic functions that generate two distinct branches.

The MCE was determined in terms of the magnetic entropy change (ΔS_M) from the magnetization measurements as a function of the applied magnetic field at different temperatures. According to the classical thermodynamic theory based on Maxwell relations, ΔS_M can be estimated via the formula:

$$\Delta S_M(T, \mu_0 H) = S_M(T, \mu_0 H) - S_M(T, 0) = \int_0^{\mu_0 H} \left(\frac{\partial M}{\partial T} \right)_{\mu_0 H} d(\mu_0 H) \quad (5)$$

where $\mu_0 H_{max}$ is the maximal value of the magnetic applied field. In practice, the relation is approximated as:

$$-\Delta S_M = \sum_i \frac{M_i - M_{i+1}}{T_{i+1} - T_i} \mu_0 \Delta H_i \quad (6)$$

where M_i and M_{i+1} are the experimental values of magnetization measured at temperatures T_i and

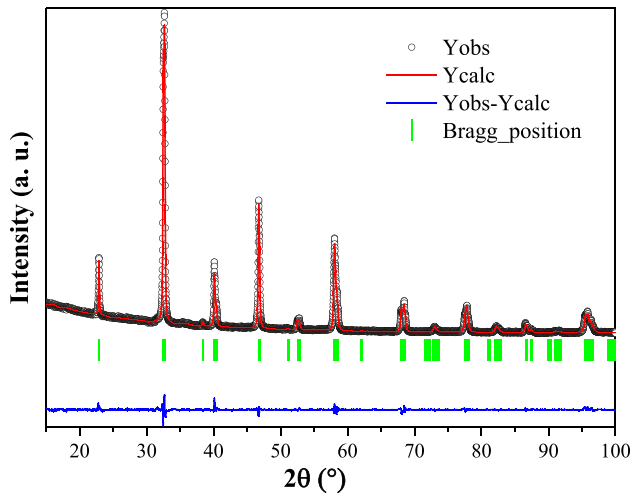


Fig. 1 XRD patterns and Rietveld refinement of $\text{La}_{0.8}\text{K}_{0.175}\text{Li}_{0.025}\text{MnO}_3$ compound

T_{i+1} respectively, under applied magnetic field change $\mu_0\Delta H_i$ [35, 36].

3 Results and discussion

3.1 Structural and microstructural properties

XRD pattern at room temperature of the $\text{La}_{0.8}\text{K}_{0.175}\text{Li}_{0.025}\text{MnO}_3$ elaborated sample, recorded at room temperature has been indexed in the rhombohedral system within the $R\bar{3}c$ space group. The compound is pure, without any evidence of impurity. The structural parameters were refined by Rietveld's profile-fitting method. The two experimental and refined XRD patterns are shown in Fig. 1. The atomic positions are situated at 6a (0, 0, 1/4) site for (La, K, Li), 6b (0, 0, 0) site for Mn and 18e (0.4532(8), 0, 1/4) site for O. The quality factors of the agreement between the experimental and the theoretical profiles are $R_B = 1.99$, $R_P = 14.3$ and $\chi^2 = 2.29$. The final refinement values of the structural parameters along with literature comparison are summarized in Table 1. The values of Mn–O bond length and the Mn–O–Mn bond angle are used to determine the bandwidth (W)

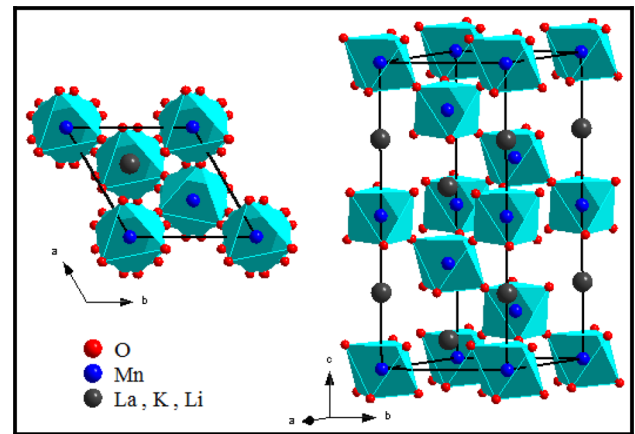


Fig. 2 The crystal structure of the rhombohedral $\text{La}_{0.8}\text{K}_{0.175}\text{Li}_{0.025}\text{MnO}_3$ sample

according to the following approximate formula [11]:

$$W \approx \frac{\cos\left[\frac{1}{2}(\pi - \langle\theta_{\text{Mn-O-Mn}}\rangle)\right]}{(d_{\text{Mn-O}})^{3.5}} \quad (7)$$

We note that the obtained value (0.0941 eV) is slightly smaller than (0.0942 eV) observed for the un-substituted sample $\text{La}_{0.8}\text{K}_{0.2}\text{MnO}_3$ [30]. The unit cell representation, produced using Diamond-Crystal software, presents the atomic positions within the crystal lattice. Figure 2 exhibits the unit cell of $\text{La}_{0.8}\text{K}_{0.175}\text{Li}_{0.025}\text{MnO}_3$ compound in the rhombohedral structure. The average crystallite size (D_{XRD}) has been calculated using the Scherrer relation as follows [33]:

$$D_{\text{XRD}} = \frac{K\lambda}{\beta\cos(\theta)} \quad (8)$$

where K , λ , β and θ are the grain shape factor, the X-ray wavelength, the full width at half maximum (FWHM) of the diffraction peak and the Bragg diffraction angle, respectively. The instrumental broadening has been taken into consideration during the FWHM calculating ($\beta = \sqrt{\beta_{\text{measured}}^2 - \beta_{\text{instrumental}}^2}$) [33]. The value of the crystallite size is equal to 43.32 nm.

The morphology and grain size have been determined by SEM. The SEM image of $\text{La}_{0.8}\text{K}_{0.175}\text{Li}_{0.025}\text{MnO}_3$ sample is given in Fig. 3. The almost polygonal grains

Table 1 Refined structural parameters of the $\text{La}_{0.8}\text{K}_{0.175}\text{Li}_{0.025}\text{MnO}_3$ sample compared to similar samples in the literature

Sample	Space Group	a, b (Å)	c (Å)	V (Å ³)	Mn–O (Å)	Mn–O–Mn (°)	Reference
$\text{La}_{0.8}\text{K}_{0.175}\text{Li}_{0.025}\text{MnO}_3$	R-3c	5.508(1)	13.385(7)	351.58	1.959(3)	164.90(6)	This work
$\text{La}_{0.8}\text{K}_{0.2}\text{MnO}_3$	R-3c	5.507(0)	13.388(4)	351.75	1.959(0)	164.92(2)	[30]
$\text{La}_{0.8}\text{K}_{0.15}\text{Li}_{0.05}\text{MnO}_3$	R-3c	5.511(2)	13.378(4)	351.90	1.961(4)	164.14(3)	[30]
$\text{La}_{0.8}\text{Na}_{0.2}\text{MnO}_3$	R-3c	5.504(0)	13.336(6)	349.87	1.954(5)	165.54	[37]
$\text{La}_{0.8}\text{Na}_{0.05}\text{Li}_{0.15}\text{MnO}_3$	R-3c	5.523(9)	13.344(4)	352.63	1.965(6)	162.66	[37]

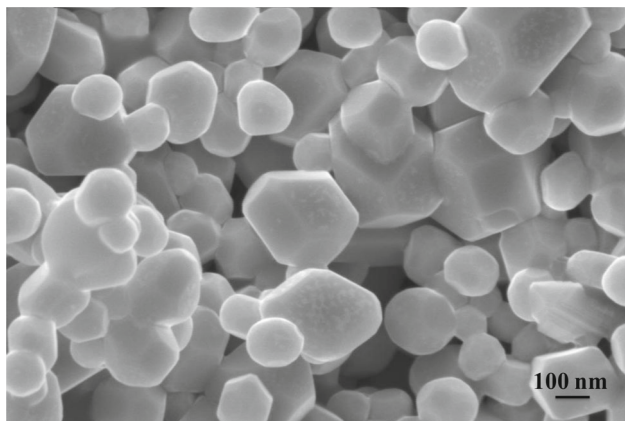


Fig. 3 SEM image of $\text{La}_{0.8}\text{K}_{0.175}\text{Li}_{0.025}\text{MnO}_3$ sample

have an average size in the sub-micrometer range ($D_{SEM} \approx 200$ nm) with inter-grain porosity. The grain sizes given by SEM (D_{SEM}) are higher than those estimated by XRD data (D_{XRD}), which indicates that every grain is composed of several crystallites [14].

3.2 Magnetic properties

Figure 4a shows the temperature dependence of magnetization $M(T)$ in zero field cooled (ZFC) and field cooled (FC) modes measured in the 5–400 K range under a magnetic applied field of 0.05 T. ZFC and FC curves exhibit a sharp paramagnetic-ferromagnetic phase transition with decreasing temperature. The T_C was determined by the minimum of the derivate dM/dT versus T curve, as shown in the inset of Fig. 4a, and is about 270 K, which is low than that of the un-substituted compound $\text{La}_{0.8}\text{K}_{0.2}\text{MnO}_3$ [30], $T_C = 287.4$ K. This difference between the two values is related to the reduction of the average ionic radius of the A-site of perovskite ($\langle r_A \rangle$) due to the partial substitution of a smaller ionic radius [37]. The reduction of T_C is additionally affected

by the narrowing of the width of the conduction bandwidth (W) diminishing from 0.0942 eV for the un-substituted sample $\text{La}_{0.8}\text{K}_{0.2}\text{MnO}_3$ to 0.0941 eV for $\text{La}_{0.8}\text{K}_{0.175}\text{Li}_{0.025}\text{MnO}_3$ sample. This involves the reduction of the overlap between the O-2p and Mn-3d orbitals, which obviously affects the double exchange interaction [38]. It is clear from Fig. 4a that our sample exhibits an irreversibility between ZFC and FC curves below T_C , which may be caused by the existence of a magnetic frustration state [39]. To obtain further information on the magnetic behavior above T_C in our nanopowder sample, the reciprocal FC magnetic susceptibility $\chi^{-1}(T)$ versus temperature is plotted in Fig. 4b. The linear change in $\chi^{-1}(T)$ in the paramagnetic phase follows the Curie–Weiss law [11, 30]:

$$\chi^{-1} = \frac{T - \theta_p}{C} \quad (9)$$

where C is the Curie constant and θ_p is the Curie–Weiss temperature. There is a downturn behavior in the $\chi^{-1}(T)$ curve above T_C . This behavior indicates the existence of the Griffiths phase which corresponds to the appearance of ferromagnetic clusters in the paramagnetic phase [40]. The temperature where the deviation of $\chi^{-1}(T)$ from Curie–Weiss linear fit started to disappear in the paramagnetic phase is called Griffiths temperature, T_G , which was deduced from the maximum of $d(1/\chi)/dT$ versus T plot (see the inset of Fig. 4b) [37]. The observed deviation of $\chi^{-1}(T)$ implied that the Curie–Weiss law was not satisfied in the temperature range between T_C and T_G ($T_C < T < T_G$) [41]. Above T_G , the Curie–Weiss law was well-obeyed, indicating typical paramagnetic behavior [42]. The values of θ_p and T_G are found to be 273.2 and 309.9 K, respectively. Moreover, the value of θ_p , which is higher than T_C for our compound, further verified the presence of magnetic inhomogeneities above T_C [37]. The Curie–Weiss analysis of the data above T_C resulted in an effective paramagnetic moment μ_{eff}^{exp} of $5.46 \mu_B$

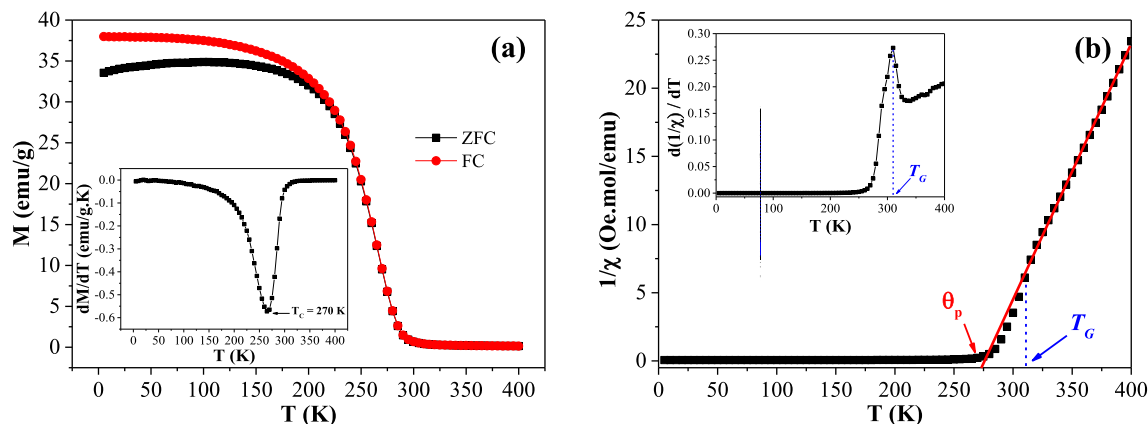


Fig. 4 Temperature dependence of the ZFC and FC magnetization (a) and the reciprocal magnetic susceptibility (b) of $\text{La}_{0.8}\text{K}_{0.175}\text{Li}_{0.025}\text{MnO}_3$ measured at 0.05 T

higher than the theoretical value of $4.52 \mu_B$, indicating the presence of a short-range magnetic order in the paramagnetic phase [39].

The magnetic field dependence of magnetization $M(H)$ up to 5 T at several temperatures between 160 and 330 K was also measured (see Fig. 5). Below T_C , the magnetization rises steeply below 0.5 T and tends to saturation for higher magnetic fields, which confirms, at low temperatures, that our elaborated compound exhibits a ferromagnetic behavior.

3.3 Critical magnetization

According to the Banerjee criterion [43], our sample exhibits, around T_C , a second-order ferromagnetic to paramagnetic phase transition with a positive slope of the M^2 vs. $\mu_0 H/M$ curves (see Fig. 6a). To analyse the nature of the second-order magnetic phase transition of $\text{La}_{0.8}\text{K}_{0.175}\text{Li}_{0.025}\text{MnO}_3$ sample, it is necessary to estimate the critical exponents β , γ and δ near the T_C . In initial, the evaluated value of T_C can be done by the modified Arrott plots (MAP) method [44] using the Arrott-Noakes equation of state:

$$(\mu_0 H/M)^{1/\gamma} = a(T - T_C)/T + bM^{1/\beta} \quad (10)$$

where a and b are constants, based on the different theoretical models: mean-field model ($\beta = 0.5$, $\gamma = 1$), tricritical mean field model ($\beta = 0.25$, $\gamma = 1$), 3D-Ising model ($\beta = 0.325$, $\gamma = 1.241$) and 3D-Heisenberg model ($\beta = 0.365$, $\gamma = 1.336$) (see Fig. 6).

As shown, all the models apart from the tricritical mean field model exhibit nearly straight lines and quasi-parallel in the high magnetic field region. In order to compare these results and choose the better model, which describes the magnetic phase transition, their relative slopes (RS) defined by $RS = S(T)/S(T_C)$. In the most ideal case, the RS should be equal to unity [45]. As the closest model, the mean field model is selected for the estimated critical exponents (see Fig. 7). Subsequent to a standard procedure in the high magnetic field region, the $M_S(T)$ and $\chi_0^{-1}(T)$ values (see Fig. 8a) are extracted from a linear extrapolation of the MAP to the intercept with the $M^{1/\beta}$ and $(\mu_0 H/M)^{1/\gamma}$ axes, respectively. The power law adjustment of the experimental data (see Fig. 8a), using Eqs. (1) and (2), leads to the estimated new values of β and γ with the corresponding T_C (see Table 2).

Additionally, the critical exponents and the T_C can be also obtained by the Kouvel-Fisher method (KF) [49]. This method is known to permit a more accurate estimation of the critical exponents based on:

$$M_S(T)[dM_S(T)/dT]^{-1} = (T - T_C)/\beta, \quad (11)$$

$$\chi_0^{-1}(T)[d\chi_0^{-1}(T)/dT]^{-1} = (T - T_C)/\gamma. \quad (12)$$

According to Eqs. (11) and (12), the plots of $M_S(T)[dM_S(T)/dT]^{-1}$ and $\chi_0^{-1}(T)[d\chi_0^{-1}(T)/dT]^{-1}$

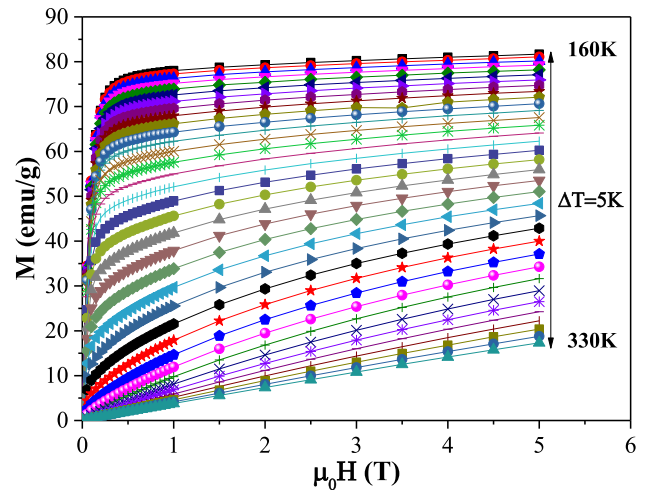


Fig. 5 Isothermal magnetization at different temperatures for $\text{La}_{0.8}\text{K}_{0.175}\text{Li}_{0.025}\text{MnO}_3$ compound

versus temperature are given in Fig. 8b. These curves should yield straight lines with slopes $1/\beta$ and $1/\gamma$, respectively, and the intercepts on temperature axes should be the T_C . The obtained critical exponents and T_C values are also listed in Table 2. Obviously, these new values are in good agreement with those estimated from the MAP.

For the third critical exponent δ , it can be estimated from the critical isotherm magnetization $M(T_C, \mu_0 H)$ (see Fig. 9) by using Eq. (3). The $\ln(M)$ vs. $\ln(\mu_0 H)$ plot should be straight line with slope $1/\delta$ at T_C (see the inset of Fig. 9). The critical exponent δ can be verified from the Windom scaling relation [50]:

$$\delta = 1 + \frac{\gamma}{\beta} \quad (13)$$

In our investigation, as a consequence δ is equal to 3.188 and 3.089 obtained from MAP and KF methods, respectively. The obtained value of δ is close to the estimate from the critical isotherm at T_C (see Table 2). Thus, the estimates of the critical exponents are compatible.

Besides, the reliability of the obtained values of the critical exponents can be checked with the prediction of the scaling hypothesis in the critical region by using Eq. (4). Using the values of β and γ obtained by MAP and KF methods, the $M|\varepsilon|^{-\beta}$ vs. $\mu_0 H|\varepsilon|^{-(\beta+\gamma)}$ plots are given in Fig. 10. The plots represent temperatures above and below T_C and the insets show the same plots in $\ln - \ln$ scale. It is clear from this last figure that all experimental points fall on two separate universal curves above and below the critical temperature, indicating the reliability of the estimation critical exponents and T_C .

Table 2 represents a comparison of the values of the critical exponents of $\text{La}_{0.8}\text{K}_{0.175}\text{Li}_{0.025}\text{MnO}_3$ compound with those of theoretical models and of other perovskite manganites reported in the literature. The

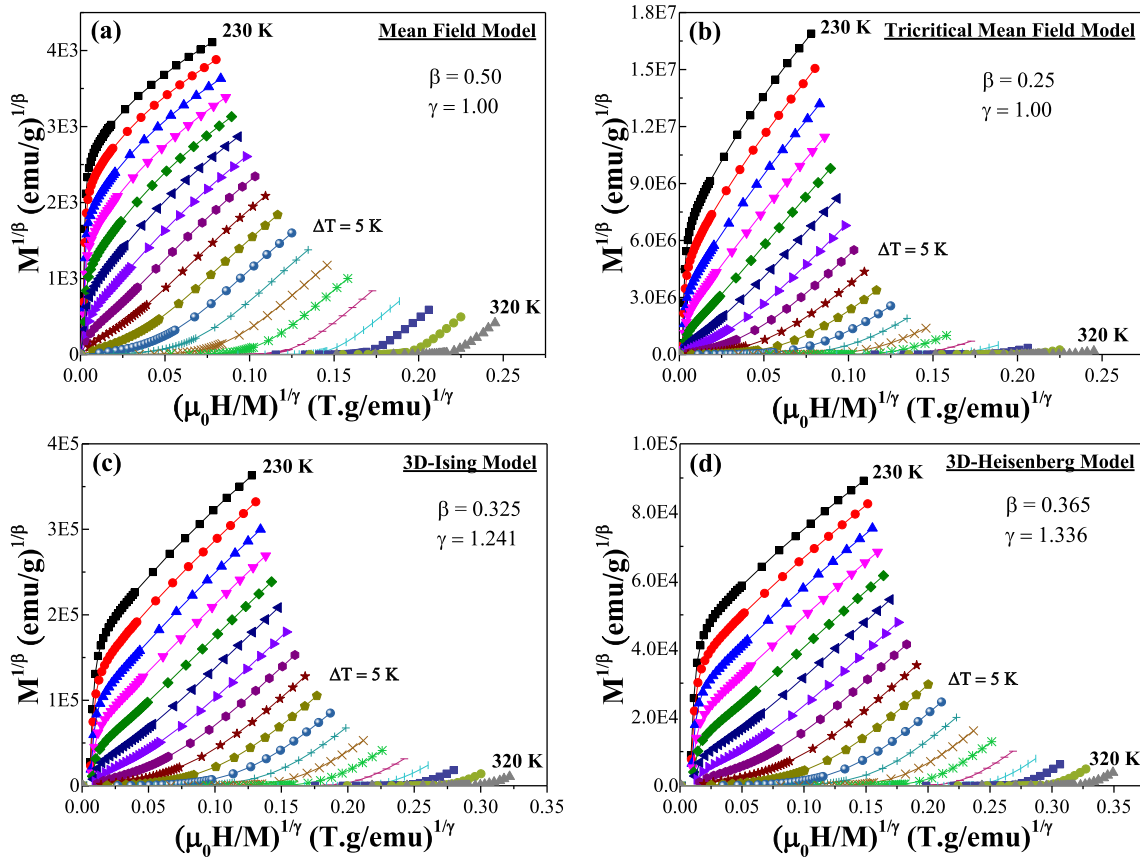


Fig. 6 Modified Arrott plots $M^{1/\beta}$ vs. $(\mu_0 H/M)^{1/\gamma}$ for $\text{La}_{0.8}\text{K}_{0.175}\text{Li}_{0.025}\text{MnO}_3$ sample using the different theoretical models

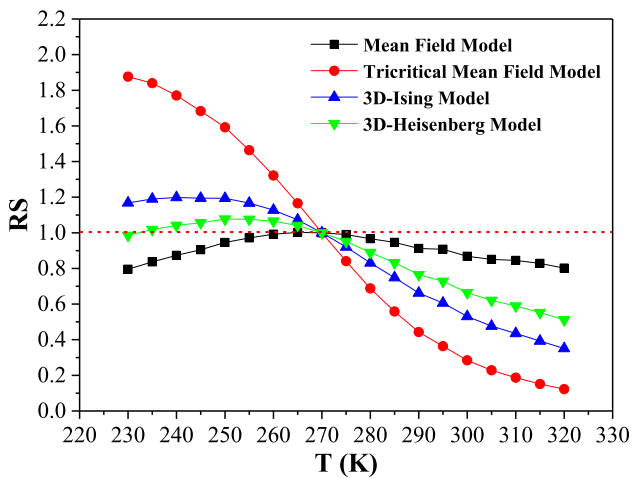


Fig. 7 Relative slope (RS) as a function of temperature for $\text{La}_{0.8}\text{K}_{0.175}\text{Li}_{0.025}\text{MnO}_3$ compound

experimental estimation values of the critical exponents of our synthesized sample are in agreement with those predicted by the mean-field model indicating that the magnetic exchange interactions in this class of materials are of the long-range type. A similar behavior has been reported for the parent sample $\text{La}_{0.8}\text{K}_{0.2}\text{MnO}_3$

[8]. Therefore, the partial replacement of potassium by lithium in the A-site of perovskite does not change the universality class of the mean-field model.

3.4 Magnetocaloric effect and its characteristics near the critical point

By using Eq. (6), the magnetic entropy change $-\Delta S_M(T, \mu_0 \Delta H)$ for $\text{La}_{0.8}\text{K}_{0.175}\text{Li}_{0.025}\text{MnO}_3$ sample was plotted (see Fig. 11). Clearly, $-\Delta S_M$ presents a peak around T_C and increases with an increasing magnetic field change $\mu_0 \Delta H$. The maximum of the magnetic entropy change $-\Delta S_M^{Max}$ is equal to $3.51 \text{ J kg}^{-1} \text{ K}^{-1}$ for a magnetic field change of 5 T.

The MCE efficiency is evaluated in terms of the relative cooling power $RCP(S)$ as:

$$RCP(S) = -\Delta S_M^{Max}(T, \mu_0 \Delta H) * \delta T_{FWHM} \quad (14)$$

where δT_{FWHM} is the full-width at half-maximum of $|\Delta S_M|$ vs. T curve [51]. According to Table 3, our elaborated sample has comparable or even higher values of magnetocaloric parameters than other magnetic materials. Further, the $RCP(S)$ value at 5 T represents about 78% of that of standard gadolinium (Gd) [2], make the present sample a very promising candidate for magnetic refrigeration [55].

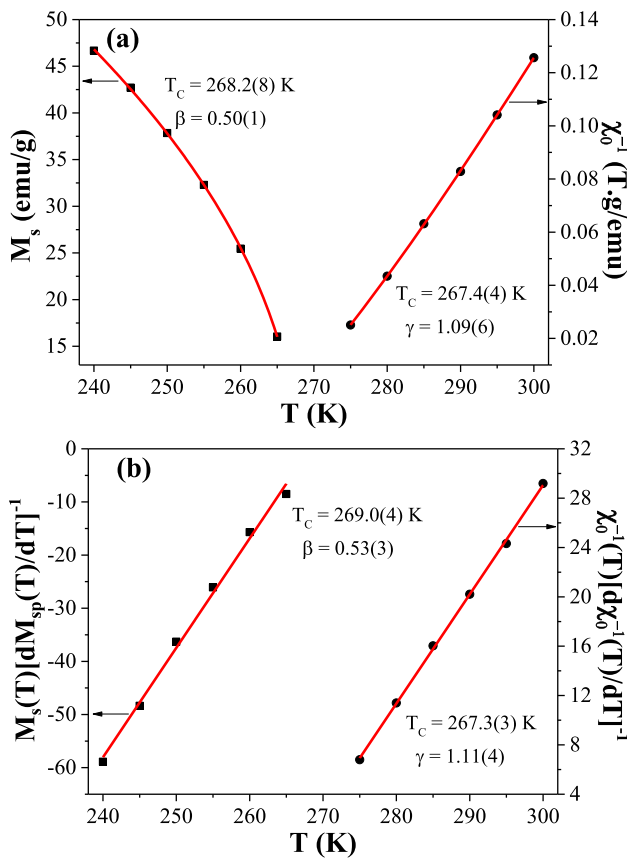


Fig. 8 Spontaneous magnetization $M_S(T)$ and inverse magnetic susceptibility $\chi_0^{-1}(T)$ versus temperature (a), and the Kouvel-Fisher plots (b) for $\text{La}_{0.8}\text{K}_{0.175}\text{Li}_{0.025}\text{MnO}_3$ sample

To reveal the correlation between the critical behavior and the MCE, near the second-order magnetic phase transition, the magnetic field dependence of the magnetic entropy change at T_C can be expressed as follows [56]:

$$-\Delta S_M^{Max} \approx a(\mu_0 \Delta H)^n \tag{15}$$

where a is a constant and n is an exponent related to the magnetic state and depends on the magnetic field and temperature. On the basis of a mean field model, the field dependence of the $-\Delta S_M$ at T_C corresponds to $n = 2/3$ [57]. With the help of the Arrott-Noakes equation of state, a new relationship between the exponent n at T_C and the critical exponents has been established as [58]:

$$n(T_C) = \left(\frac{\beta - 1}{\beta + \gamma} \right) + 1 = 1 + \frac{1}{\delta} \left(1 - \frac{1}{\beta} \right) \tag{16}$$

As shown in Fig. 12, the $-\Delta S_M^{Max}$ vs. $\mu_0 \Delta H$ curve exhibits a monotone increase which indicates the magnetic transition from ferromagnetic to paramagnetic phases [30]. However, note that the value of $n = 0.85$ at T_C reveals an obvious deviation from $n \approx 0.66$ for the mean field model. Furthermore, using β and γ estimated from the above discussion, the value of n is calculated to be 0.68 and 0.71 for MAP and KF methods, respectively. The slight discrepancy between the determined n and that obtained from the MAP method is due to the presence of local inhomogeneities in vicinity of the magnetic phase transition [59, 60].

Moreover, Franco et al. [61] have proposed that the $\Delta S_M(T)$ curves recorded with various magnetic field changes may collapse into a single universal scaling curve when properly rescaled. This process is achieved

Table 2 The critical exponent's values of $\text{La}_{0.8}\text{K}_{0.175}\text{Li}_{0.025}\text{MnO}_3$ sample compared to values reported in the literature. Abbreviations: MAP, modified Arrott plots; KF, Kouvel-Fisher; CI, Critical Isotherm; cal, calculated and exp, experimental

Material	Method	T_C (K)	β	γ	δ	Reference
Mean field model	Theory		0.5	1	3	[28]
3D-Heisenberg model	Theory		0.365	1.336	4.80	[28]
3D-Ising model	Theory		0.325	1.241	4.82	[28]
Tricritical mean field model	Theory		0.25	1	5	[29]
$\text{La}_{0.8}\text{K}_{0.175}\text{Li}_{0.025}\text{MnO}_3$	MAP	267.86	0.501	1.096	3.188 (cal)	This work
	KF	268.18	0.533	1.114	3.089 (cal)	
	CI	270			2.965 (exp)	
$\text{La}_{0.8}\text{K}_{0.2}\text{MnO}_3$	MAP	332.3	0.720	1.100	2.527	[8]
$\text{La}_{0.8}\text{K}_{0.2}\text{MnO}_3$	KF	332.28	0.630	1.040	2.650	[8]
$\text{La}_{0.6}\text{Dy}_{0.1}\text{Sr}_{0.3}\text{MnO}_3$	MAP	307	0.479	1.374	3.863	[22]
$\text{La}_{0.7}\text{Sr}_{0.3}\text{Mn}_{0.8}\text{Ti}_{0.2}\text{O}_3$	MAP	150.1	0.518	1.008	2.950	[46]
$\text{La}_{0.7}\text{Sr}_{0.3}\text{Mn}_{0.95}\text{Al}_{0.05}\text{O}_3$	KF	336.24	0.458	1.001	3.185	[47]
$\text{La}_{0.67}\text{Ba}_{0.22}\text{Sr}_{0.11}\text{Mn}_{0.9}\text{Ti}_{0.1}\text{O}_3$	MAP	258.03	0.516	1.375	3.664	[48]
$\text{La}_{0.67}\text{Ba}_{0.22}\text{Sr}_{0.11}\text{Mn}_{0.9}\text{Ti}_{0.1}\text{O}_3$	KF	260.12	0.498	1.214	3.437	[48]

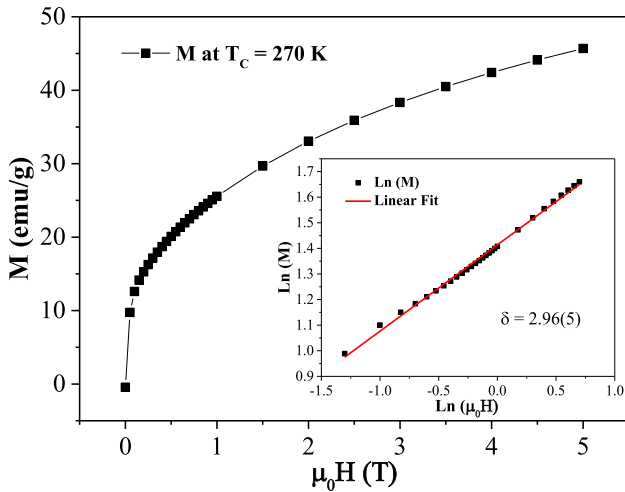


Fig. 9 Isothermal magnetization $M(\mu_0H)$ at T_C . Inset shows the $\text{Ln} - \text{Ln}$ scale plot

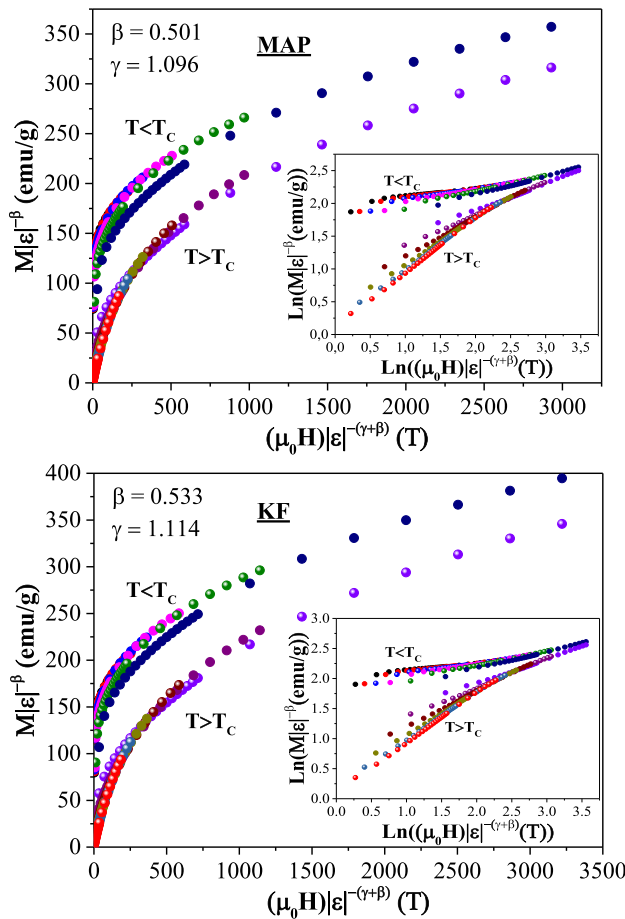


Fig. 10 Scaling plots of $M|\varepsilon|^{-\beta}$ vs. $\mu_0H|\varepsilon|^{-(\beta+\gamma)}$ above and below T_C for $\text{La}_{0.8}\text{K}_{0.175}\text{Li}_{0.025}\text{MnO}_3$ compound. The insets show the same plots on a $\text{Ln} - \text{Ln}$ scale

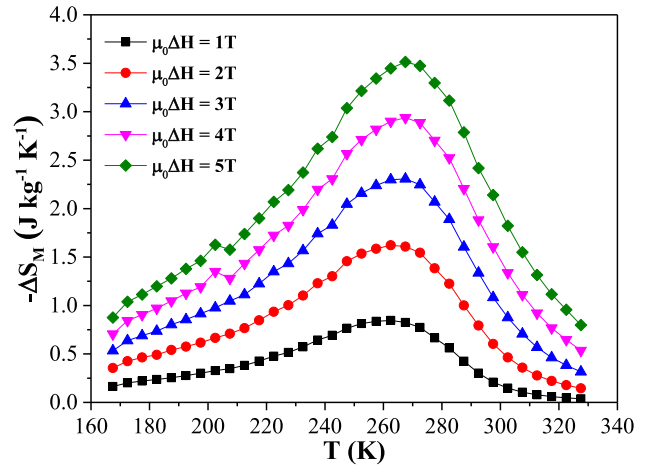


Fig. 11 Temperature dependence of magnetic entropy change $-\Delta S_M$ for different magnetic field changes for $\text{La}_{0.8}\text{K}_{0.175}\text{Li}_{0.025}\text{MnO}_3$ sample

by normalizing all the $\Delta S_M(T)$ curves using their specific maximum value (ΔS_M^{Max}), namely, $\Delta S' = \Delta S_M / \Delta S_M^{Max}$ and then rescaling the temperature axis above and below T_C as expressed in Eq. (17):

$$\theta = \begin{cases} -(T - T_C)/(T_{r1} - T_C), & T \leq T_C \\ (T - T_C)/(T_{r2} - T_C), & T > T_C \end{cases} \quad (17)$$

where T_{r1} and T_{r2} are the temperatures chosen such that $\Delta S_M(T_{r1,2}) = \Delta S_M^{Max}/2$. As can be noted from Fig. 13 for $\text{La}_{0.8}\text{K}_{0.175}\text{Li}_{0.025}\text{MnO}_3$ sample, all experimental data collapse onto a single universal curve revealing second order phase transition.

Additionally to confirm the reliability of the obtained critical exponents, the scaling hypothesis, making a single universal scaling curve for all measured fields and temperatures [60], should be tested as:

$$-\Delta S_M(\mu_0H, T) = (\mu_0H)^{(1-\alpha)/(\beta+\gamma)} f\left[\varepsilon/(\mu_0H)^{1/(\beta+\gamma)}\right] \quad (18)$$

where $\alpha = 2 - 2\beta - \gamma$ is the critical exponent and $\varepsilon = (T - T_C)/T_C$ is the reduced temperature. We plotted the scaled magnetic entropy change versus scaled temperature employing the obtained critical exponents using Eq. (18). As shown in Fig. 14, all experimental data collapse on a single universal curve for different fields and temperatures, which again confirms a good correlation between the obtained critical exponents and the MCE. We observed slight discrepancies at $T < T_C$, indicating the nonlinear behavior of the $\text{La}_{0.8}\text{K}_{0.175}\text{Li}_{0.025}\text{MnO}_3$ compound caused by the competing exchange interactions and the structural inhomogeneity [60].

Table 3 Experimental values of T_C (estimated from the $M(T)$ data), $-\Delta S_M^{Max}$ and RCP for $\text{La}_{0.8}\text{K}_{0.175}\text{Li}_{0.025}\text{MnO}_3$ compound compared with those of other perovskite manganites and of Gd

Material	T_C (K)	$\mu_0\Delta H$ (T)	$-\Delta S_M^{Max}$ (J/kgK)	RCP (J/kg)	Reference
$\text{La}_{0.8}\text{K}_{0.175}\text{Li}_{0.025}\text{MnO}_3$	270	1	0.84	59.7	This work
		2	1.62	125.3	
		3	2.30	188.5	
		4	2.93	251.6	
		5	3.51	320.5	
$\text{La}_{0.7}\text{Sr}_{0.2}\text{Li}_{0.1}\text{MnO}_3$	272.3	2	1.07	83.2	[11]
$\text{La}_{0.7}\text{Sr}_{0.15}\text{Li}_{0.15}\text{MnO}_3$	194.4	2	1.00	102.5	[11]
$\text{La}_{0.8}\text{K}_{0.2}\text{MnO}_3$	287.4	2	1.57	88.8	[30]
$\text{La}_{0.65}\text{Dy}_{0.05}\text{Sr}_{0.3}\text{MnO}_3$	265	2	0.86	80.0	[52]
$\text{La}_{0.8}\text{Ca}_{0.15}\text{Na}_{0.05}\text{MnO}_3$	245	2	4.6	89	[53]
$\text{La}_{0.8}\text{Na}_{0.2}\text{Mn}_{0.97}\text{Ni}_{0.03}\text{O}_3$	275	5	3.7	251	[54]
$\text{La}_{0.8}\text{Na}_{0.2}\text{Mn}_{0.94}\text{Ni}_{0.06}\text{O}_3$	257	5	3.7	258	[54]
$\text{La}_{0.8}\text{Ag}_{0.2}\text{MnO}_3$	278.5	5	6.12	217.8	[15]
Gd	294	5	10.20	410.0	[2]

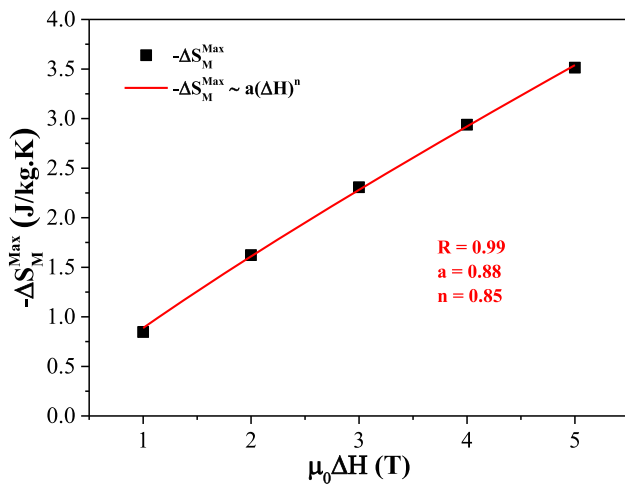


Fig. 12 Field dependence of $-\Delta S_M^{Max}$ for $\text{La}_{0.8}\text{K}_{0.175}\text{Li}_{0.025}\text{MnO}_3$ compound

4 Conclusion

In summary, the $\text{La}_{0.8}\text{K}_{0.175}\text{Li}_{0.025}\text{MnO}_3$ sample was elaborated by the sol-gel method at low temperature. Our sample crystallizes in the rhombohedral structure within the $R\bar{3}c$ space group. Magnetic measurements showed that our investigated compound undergoes a second-order paramagnetic-ferromagnetic transition at a $T_C \sim 270$ K. The values of the maximum of the mag-

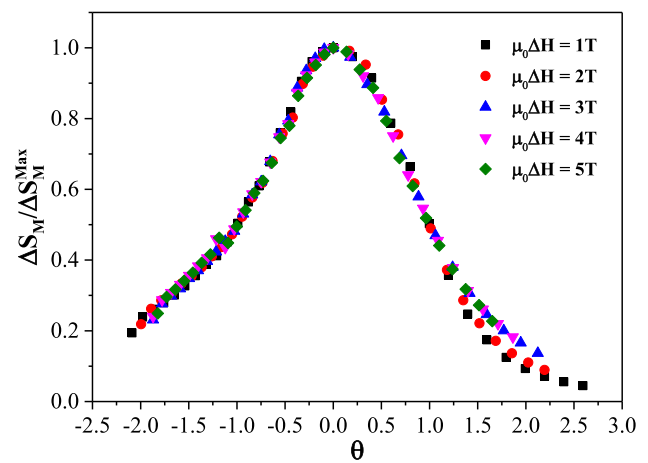


Fig. 13 Universal behavior of the scaled magnetic entropy change curves of $\text{La}_{0.8}\text{K}_{0.175}\text{Li}_{0.025}\text{MnO}_3$ sample

netic entropy change $-\Delta S_M^{Max}$ and the relative cooling power $RCP(S)$ are large sufficient for it to be used in magnetic refrigeration. The critical exponents β , γ and δ , are estimated using the modified Arrott plot and Kouvel-Fisher methods and close to the mean field model. The magnetic entropy change could be characterized by a single universal curve using the scaling hypothesis.

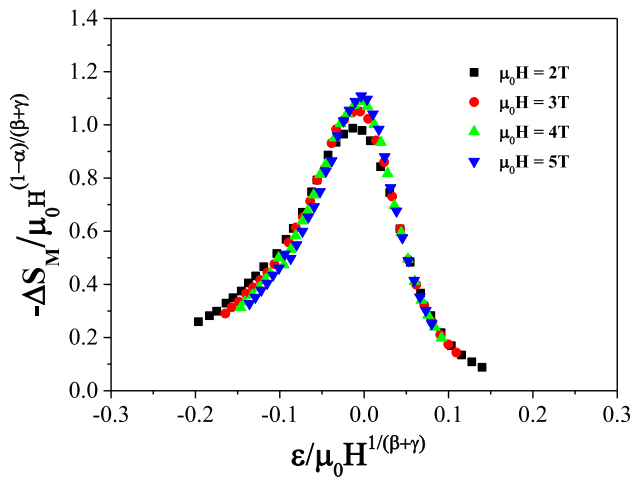


Fig. 14 Scaled magnetic entropy change versus scaled temperature for $\text{La}_{0.8}\text{K}_{0.175}\text{Li}_{0.025}\text{MnO}_3$ compound

Acknowledgements This study has been supported by the Tunisian Ministry of Higher Education and Scientific Research.

Author contribution statement

YR: materials preparation, Conceptualization, data collection, analysis, Writing—review & editing. WC-K: Formal analysis and interpretation of data. LS: Formal analysis and technical discussion. EKH: Formal analysis and technical discussion. All authors discussed the results and reviewed the manuscript.

Data availability statement Data will be made available on reasonable request.

References

1. V. Franco, J.S. Blázquez, J.J. Ipus, J.Y. Law, L.M. Moreno-Ramírez, A. Conde, Magnetocaloric effect: from materials research to refrigeration devices. *Prog. Mater. Sci.* **93**, 112–232 (2018). <https://doi.org/10.1016/j.pmatsci.2017.10.005>
2. K.A. Gschneider Jr., V.K. Pecharsky, A.O. Tsokol, Recent developments in magnetocaloric materials. *Rep. Prog. Phys.* **68**, 1479–1539 (2005). <https://www.doi.org/https://doi.org/10.1088/0034-4885/68/6/R04>
3. V.K. Pecharsky, K.A. Gschneider Jr., Giant magnetocaloric effect in $\text{Gd}_5(\text{Si}_2\text{Ge}_2)$. *Phys. Rev. Lett.* **78**, 4494 (1997). <https://doi.org/10.1103/PhysRevLett.78.4494>
4. V. Franco, J.S. Blázquez, B. Ingale, A. Conde, The magnetocaloric effect and magnetic refrigeration near room temperature: materials and models. *Annu. Rev. Mater. Res.* **42**, 305–342 (2012). <https://doi.org/10.1146/annurev-matsci-062910-100356>
5. Y. Regaieg, F. Ayadi, J. Monnier, S. Reguer, M. Koubaa, A. Cheikhrouhou, S. Nowak, L. Sicard, S. Ammar-Merah, Magnetocaloric properties of $\text{La}_{0.67}\text{Ca}_{0.33}\text{MnO}_3$ produced by reactive spark plasma sintering and by conventional ceramic route. *Mater. Res. Express* **1**, 046105 (2014). <http://iopscience.iop.org/2053-1591/1/4/046105/article?fromSearchPage=true>
6. M. Ben Rejeb, C. Ben Osman, Y. Regaieg, A. Marzouki-Ajmi, W. Cheikhrouhou-Koubaa, S. Ammar-Merah, A. Cheikhrouhou, T. Mhiri, A comparative study of $\text{La}_{0.65}\text{Ca}_{0.2}(\text{Na}_{0.5}\text{K}_{0.5})_{0.15}\text{MnO}_3$ compound synthesized by solid-state and sol-gel process. *J. Alloys Comp.* **695**, 2597–2604 (2017). <https://doi.org/10.1016/j.jallcom.2016.11.166>
7. V.E. Salazar-Munoz, S.A. Palomares-Sanchez, I. Betancourt, A.A. Torres-Castillo, J. G. Cabal Velarde, A. Lobo Guerrero, Magnetic and magnetocaloric properties of a foam composite based on substituted Lammanganite in a polyurethane matrix. *J. Magn. Mater.* **538**, 168296 (2021). <https://doi.org/10.1016/j.jmmm.2021.168296>
8. R. Skini, H. Baaziz, A. Tozri, M. Abdel-Hafiez, A. Hassan, Magnetocaloric effect and critical behavior in $\text{La}_{0.8}\text{K}_{0.2}\text{MnO}_3$ nanoparticle. *Results Phys.* **30**, 104861 (2021). <https://doi.org/10.1016/j.rinp.2021.104861>
9. K. Laajimi, M. Kchaw, I. Fourati, J. Juraszek, M. H. Gazzah, J. Dhahri, Large magnetocaloric effect in $0.25(\text{La}_{0.67}\text{Ca}_{0.33}\text{MnO}_3 + \text{La}_{0.67}\text{Ca}_{0.13}\text{Sr}_{0.2}\text{Mn}_{0.98}\text{Ni}_{0.02}\text{O}_3)_{0.5}\text{La}_{0.67}\text{Ca}_{0.23}\text{Sr}_{0.1}\text{Mn}_{0.98}\text{Ni}_{0.02}\text{O}_3$ composite close to room temperature. *Eur. Phys. J. Plus* **137**, 943 (2022). <https://doi.org/10.1140/epjp/s13360-022-03153-0>
10. Z. Gong, W. Xu, N.A. Liedienov, D.S. Butenko, I.V. Zatonvsky, I.A. Gural'skiy, Z. Wei, Q. Li, B. Liu, Y.A. Batman, A.V. Pashchenko, G.G. Levchenko, Expansion of the multifunctionality in off-stoichiometric manganites using post-annealing and high pressure: physical and electrochemical studies. *Phys. Chem. Chem. Phys.* **24**, 21872–21885 (2022). <https://doi.org/10.1039/D2CP01959K>
11. I. Othmani, Y. Regaieg, F. Ayadi, W. Cheikhrouhou-Koubaa, M. Koubaa, V. Nachbaur, M. Abdelhedi, A. Cheikhrouhou, Effect of lithium substitution on the structural, magnetic and magnetocaloric properties of $\text{La}_{0.7}\text{Sr}_{0.3-x}\text{Li}_x\text{MnO}_3$ ($0 \leq x \leq 0.15$). *J. Supercond. Nov. Magn.* **36**, 1143–1152 (2023). <https://doi.org/10.1007/s10948-023-06554-z>
12. H. Yu, N. Liedienov, I. Zatonvsky, D. Butenko, I. Fesych, W. Xu, C. Song, Q. Li, B. Liu, A. Pashchenko, G. Levchenko, The multifunctionality of lanthanum-strontium cobaltite nanopowder: high-pressure magnetic studies and excellent electrocatalytic properties for OER. *ACS Appl. Mater. Interfaces* **16**, 3605–3620 (2024). <https://doi.org/10.1021/acsami.3c06413>
13. D. Su, N.A. Liedienov, V.M. Kalita, I.V. Fesych, W. Xu, A.V. Bodnaruk, Y.I. Dzhzherya, Q. Li, B. Liu, G.G. Levchenko, Structural size effect-, aging time-, and pressure-dependent functional properties of Mn-containing perovskite nanoparticles. *Acta Mater.* **280**, 120332 (2024). <https://doi.org/10.1016/j.actamat.2024.120332>

14. M. Soleymani, A. Moheb, E. Joudaki, High surface area nano-sized $\text{La}_{0.6}\text{Ca}_{0.4}\text{MnO}_3$ perovskite powder prepared by low temperature pyrolysis of a modified citrate gel. *Cent. Eur. J. Chem.* **7**, 809–817 (2009). <https://doi.org/10.2478/s11532-009-0083-2>
15. Y. Regaieg, M. Koubaa, W. Cheikhrouhou-Koubaa, A. Cheikhrouhou, L. Sicard, S. Ammar-Merah, F. Herbst, Structure and magnetocaloric properties of $\text{La}_{0.8}\text{Ag}_{0.2-x}\text{K}_x\text{MnO}_3$ perovskite manganites. *Mater. Chem. Phys.* **132**, 839–845 (2012). <https://doi.org/10.1016/j.matchemphys.2011.12.021>
16. F. Ayadi, S. Ammar, S. Nowak, W. Cheikhrouhou-Koubaa, Y. Regaieg, M. Koubaa, J. Monnier, L. Sicard, Importance of the synthesis and sintering methods on the properties of manganese ceramics: The example of $\text{La}_{0.7}\text{Ca}_{0.3}\text{MnO}_3$. *J. Alloys Comp.* **759**, 52–59 (2018). <https://doi.org/10.1016/j.jallcom.2018.05.113>
17. I.Z. Al-Yahmadi, A.M. Gismelseed, F. Al Ma'Mari, A.D. Al-Rawas, S.H. Al-Harthi, A.Y. Yousif, H.M. Widatalah, M.E. Elzain, M.T.Z. My, Structural, magnetic and magnetocaloric effect studies of $\text{Nd}_{0.6}\text{Sr}_{0.4}\text{A}_x\text{Mn}_{1-x}\text{O}_3$ (A=Co, Ni, Zn) perovskite manganites. *J. Alloys Comp.* **875**, 159977 (2021). <https://doi.org/10.1016/j.jallcom.2021.159977>
18. C. Zener, Interaction between the d-shells in the transition metals. II. Ferromagnetic compounds of manganese with perovskite structure. *Phys. Rev.* **82**, 403–405 (1951). <https://doi.org/10.1103/PhysRev.82.403>
19. M.H. Phan, S.B. Tian, D.Q. Hoang, S.C. Yu, C. Nguyen, A.N. Ulyanov, Large magnetic-entropy change above 300K in CMR materials. *J. Magn. Magn. Mater.* **309**, 258–259 (2003). [https://doi.org/10.1016/S0304-8853\(02\)01151-4](https://doi.org/10.1016/S0304-8853(02)01151-4)
20. S.L. Yuan, Z.C. Xia, L. Liu, W. Chen, L.F. Zhao, J. Tang, G.H. Zhang, L.J. Zhang, H. Cao, W. Feng, Y. Tian, L.Y. Niu, S. Liu, Electrical transport in manganite granular systems. *Phys. Rev. B* **68**, 184423 (2003). <https://doi.org/10.1103/PhysRevB.68.184423>
21. J. Fan, L. Pi, L. Zhang, W. Tong, L. Ling, B Hong, Y. Shi, W. Zhang, D. Lu, Y. Zhang, Investigation of critical behavior in $\text{Pr}_{0.55}\text{Sr}_{0.45}\text{MnO}_3$ by using the field dependence of magnetic entropy change. *Appl. Phys. Lett.* **98**, 072508 (2011). <https://doi.org/10.1063/1.3554390>
22. L. Xu, L. Chen, J. Fan, K. Bärner, L. Zhang, Y. Zhu, L. Pi, Y. Zhang, D. Shi, Room-temperature large magnetocaloric effect and critical behavior in $\text{La}_{0.6}\text{Dy}_{0.1}\text{Sr}_{0.3}\text{MnO}_3$. *Ceram. Int.* **42**, 8234–8239 (2016). <https://doi.org/10.1016/j.ceramint.2016.02.035>
23. N.A. Liedienov, V.M. Kalita, A.V. Pashchenko, Y.I. Dzhezherya, I.V. Fesych, Q. Li, G.G. Levchenko, Critical phenomena of magnetization, magnetocaloric effect, and superparamagnetism in nanoparticles of non-stoichiometric manganite. *J. Alloys Comp.* **836**, 155440 (2020). <https://doi.org/10.1016/j.jallcom.2020.155440>
24. D. Kim, B. Revaz, B.L. Zink, F. Hellman, J.J. Rhyne, J.F. Mitchell, Tricritical point and the doping dependence of the order of the ferromagnetic phase transition of $\text{La}_{1-x}\text{Ca}_x\text{MnO}_3$. *Phys. Rev. Lett.* **89**, 227202 (2002). <https://doi.org/10.1103/PhysRevLett.89.227202>
25. J. Mira, J. Rivsa, F. Rivadulla, C.V. Vazquez, M.A.L. Quintela, Change from first- to second-order magnetic phase transition in $\text{La}_{2/3}(\text{Ca}, \text{Sr})_{1/3}\text{MnO}_3$ perovskites. *Phys. Rev. B* **60**, 2998 (1999). <https://doi.org/10.1103/PhysRevB.60.2998>
26. H.S. Shin, J.E. Lee, Y.S. Nam, H.L. Ju, C.W. Park, First-order-like magnetic transition in manganite oxide $\text{La}_{0.7}\text{Ca}_{0.3}\text{MnO}_3$. *Solid State Commun.* **118**, 377–380 (2001). [https://doi.org/10.1016/S0038-1098\(01\)00123-5](https://doi.org/10.1016/S0038-1098(01)00123-5)
27. A.K. Pramanik, A. Banerjee, Critical behavior at paramagnetic to ferromagnetic phase transition in $\text{Pr}_{0.5}\text{Sr}_{0.5}\text{MnO}_3$: a bulk magnetization study. *Phys. Rev. B* **79**, 214426 (2009). <https://doi.org/10.1103/PhysRevB.79.214426>
28. S.N. Kaul, Static critical phenomena in ferromagnets with quenched disorder. *J. Magn. Magn. Mater.* **53**, 5–53 (1985). [https://doi.org/10.1016/0304-8853\(85\)90128-3](https://doi.org/10.1016/0304-8853(85)90128-3)
29. K. Huang, *Statistical Mechanics* (Wiley, NewYork, 1987)
30. Y. Regaieg, W. Cheikhrouhou-Koubaa, L. Sicard, S. Gam-Derouich, S. Nowak, M. Koubaa, E.K. Hlil, A. Cheikhrouhou, Structural, magnetic and magnetocaloric properties of Li-substituted $\text{La}_{0.8}\text{K}_{0.2-x}\text{Li}_x\text{MnO}_3$ perovskite manganites. *Inorg. Chim. Acta* **567**, 122065 (2024). <https://doi.org/10.1016/j.ica.2024.122065>
31. H.M. Rietveld, A profile refinement method for nuclear and magnetic structures. *J. Appl. Crystallogr.* **2**, 65–71 (1969). <https://doi.org/10.1107/S0021889869006558>
32. J. Rodriguez-Carvajal, Recent advances in magnetic structure determination by neutron powder diffraction. *Phys. B: Condens. Matter* **192**, 55–69 (1993). [https://doi.org/10.1016/0921-4526\(93\)90108-I](https://doi.org/10.1016/0921-4526(93)90108-I)
33. N. Kharrat, I.S. Debbebi, W. Cheikhrouhou-Koubaa, M. Koubaa, A. Cheikhrouhou, L. Sicard, Magnetocaloric Effect in $\text{La}_{0.67}\text{Ba}_{0.33}\text{Mn}_{0.95}\text{Ni}_{0.05}\text{O}_3$ Manganite Near Room Temperature. *J. Supercond. Nov. Magn.* **32**, 1241–1251 (2019). <https://doi.org/10.1007/s10948-018-4816-3>
34. H.E. Stanley, *Introduction to Phase Transition and Critical Phenomena* (Oxford University Press, New York, 1971)
35. A.R. Dinesen, S. Linderoth, S. Moerup, Direct and indirect measurement of the magnetocaloric effect in $\text{La}_{0.67}\text{Ca}_{0.33-x}\text{Sr}_x\text{MnO}_3 \pm \delta$ ($x \in [0: 0.33]$). *J. Phys.: Condens. Matter* **17**, 6257–6269 (2005). <https://iopscience.iop.org/article/https://doi.org/10.1088/0953-8984/17/39/011>
36. R.D. McMichael, J.J. Ritter, R.D. Shull, Enhanced magnetocaloric effect in $\text{Gd}_3\text{Ga}_{5-x}\text{Fe}_x\text{O}_{12}$. *J. Appl. Phys.* **73**, 6946–6948 (1993). <https://doi.org/10.1063/1.352443>
37. A. Zahrin, N. Ibrahim, Z. Mohamed, Effects of Li substitution on structural, magnetic properties and electroresistance behaviour in $\text{La}_{0.8}\text{Na}_{0.2-x}\text{Li}_x\text{MnO}_3$ monovalent-doped manganite. *Mater. Sci. Eng. B* **295**, 116613 (2023). <https://doi.org/10.1016/j.mseb.2023.116613>
38. A.J. Millis, P.B. Littlewood, B.I. Shraiman, Double Exchange Alone Does Not Explain the Resistivity of $\text{La}_{1-x}\text{Sr}_x\text{MnO}_3$. *Phys. Rev. Lett.* **74**, 5144–5147 (1995). <https://doi.org/10.1103/PhysRevLett.74.5144>
39. Z. Wei, N.A. Liedienov, Q. Li, A.V. Pashchenko, W. Xu, V. A. Turchenko, M. Yuan, I.V. Fesych, G.G. Levchenko, Influence of post-annealing, defect chemistry and high pressure on the magnetocaloric effect

- of non-stoichiometric $\text{La}_{0.8-x}\text{K}_{0.2}\text{Mn}_{1+x}\text{O}_3$ compounds. *Ceram. Int.* **47**(17), 24553–24563 (2021). <https://doi.org/10.1016/j.ceramint.2021.05.174>
40. Magnetic behavior and magnetocaloric properties, Y. Regaieg, L. Sicard, J. Monnier, G. Delaizir, M. Koubaa, C. Godart, S. Ammar-Merah, A. Cheikhrouhou, Rapid synthesis of $\text{La}_{0.85}\text{Na}_{0.15}\text{MnO}_3$ by spark plasma sintering. *Mater. Chem. Phys.* **139**, 629–633 (2013). <https://doi.org/10.1016/j.matchemphys.2013.02.008>
 41. N.A. Azhar, I.S. Ismail, N.B. Mohamed, A. Hashim, Z. Mohamed, Effect of Bisubstitution on structural and AC magnetic susceptibility properties of $\text{Nd}_{1-x}\text{Bi}_x\text{MnO}_3$. *Crystals* **10**(6), 1–10 (2020). <https://doi.org/10.3390/cryst10060521>
 42. M.A. Gdaiem, M. Abassi, J. Dhahri, E.K. Hlil, Structural, magnetic, magnetocaloric properties and the formation of nano-size Griffiths-like clusters in $\text{La}_{0.8}\text{Ba}_{0.1}\text{Ca}_{0.1}\text{Mn}_{0.8}\text{Co}_{0.2}\text{O}_3$ manganites. *J. Alloys Compd.* **646**, 1068–1074 (2015). <https://doi.org/10.1016/j.jallcom.2015.06.178>
 43. S.K. Banerjee, On a generalised approach to first and second order magnetic transitions. *Phys. Lett.* **12**, 16–17 (1964). [https://doi.org/10.1016/0031-9163\(64\)91158-8](https://doi.org/10.1016/0031-9163(64)91158-8)
 44. A. Arrott, J.E. Noakes, Approximate equation of state for nickel near its critical temperature. *Phys. Rev. Lett.* **19**, 786 (1967). <https://doi.org/10.1103/PhysRevLett.19.786>
 45. H. Ben Khelifa, R. M'nassri, S. Tarhouni, Y. Regaieg, W. Cheikhrouhou-Koubaa, N. Chniba-Boudjada, A. Cheikhrouhou, Critical behaviour and field dependence of magnetic entropy change in K-doped manganites $\text{Pr}_{0.8}\text{Na}_{0.2-x}\text{K}_x\text{MnO}_3$ ($x = 0.10$ and 0.15). *J. Solid State Chem.* **257**, 9–18 (2018). <https://doi.org/10.1016/j.jssc.2017.09.013>
 46. N.V. Khiem, L.V. Bau, P.T. Phong, L.V. Hong, N.V. Dai, D.N.H. Nam, N.X. Phuc, Critical Exponents for the Ferromagnetic-Paramagnetic Transition in $\text{La}_{0.7}\text{Sr}_{0.3}\text{Mn}_{0.8}\text{Ti}_{0.2}\text{O}_3$. *J. Korean Phys. Soc.* **52**, 1518–1521 (2008). <https://doi.org/10.3938/jkps.52.1518>
 47. N.V. Khiem, P.T. Phong, L.V. Bau, D.N.H. Nam, L.V. Hong, N.X. Phuc, Critical parameters near the ferromagnetic-paramagnetic phase transition in $\text{La}_{0.7}\text{A}_{0.3}(\text{Mn}_{1-x}\text{B}_x)\text{O}_3$ ($\text{A} = \text{Sr}$; $\text{B} = \text{Ti}$ and Al ; $x = 0.0$ and 0.05) compounds. *J. Magn. Magn. Mater.* **321**, 2027–2031 (2009). <https://doi.org/10.1016/j.jmmm.2009.01.011>
 48. F. Ben Jemaa, S.H. Mahmood, M. Ellouze, E.K. Hlil, F. Halouani, Structural, magnetic, magnetocaloric, and critical behavior of selected Ti-doped manganites. *Ceram. Int.* **41**, 8191–8202 (2015). <https://doi.org/10.1016/j.ceramint.2015.03.039>
 49. J.S. Kouvel, M.E. Fisher, Detailed magnetic behavior of nickel near its curie point. *Phys. Rev.* **136**, A1626 (1964). <https://doi.org/10.1103/PhysRev.136.A1626>
 50. B. Widom, Equation of state in the neighborhood of the critical point. *J. Chem. Phys.* **43**, 3898–3905 (1965). <https://doi.org/10.1063/1.1696618>
 51. K.A. Gschneidner, V.K. Pecharsky, Magnetocaloric Materials. *Annu. Rev. Mater. Sci.* **30**, 387–429 (2000). <https://doi.org/10.1146/annurev.matsci.30.1.387>
 52. R. Felhi, M. Koubaa, W. Cheikhrouhou-Koubaa, A. Cheikhrouhou, Structural, magnetic, magnetocaloric and critical behavior investigations of $\text{La}_{0.65}\text{Dy}_{0.05}\text{Sr}_{0.3}\text{MnO}_3$ manganite. *J. Alloys Compd.* **726**, 1236–1245 (2017). <https://doi.org/10.1016/j.jallcom.2017.08.080>
 53. S. Choura Maatar, R. M'nassri, W. Cheikhrouhou Koubaa, M. Koubaa, A. Cheikhrouhou, Structural, magnetic and magnetocaloric properties of $\text{La}_{0.8}\text{Ca}_{0.2-x}\text{Na}_x\text{MnO}_3$ manganites ($0 \leq x \leq 0.2$). *J. Solid State Chem.* **225**, 83–88 (2015). <https://doi.org/10.1016/j.jssc.2014.12.007>
 54. O. Hassayoun, M. Baazaoui, M.R. Laouyenne, F. Hsnib, E.K. Hlil, M. Oumezzine, Kh. Farah, Magnetocaloric effect and electron paramagnetic resonance studies of the transition from ferromagnetic to paramagnetic in $\text{La}_{0.8}\text{Na}_{0.2}\text{Mn}_{1-x}\text{Ni}_x\text{O}_3$ ($0 \leq x \leq 0.06$). *J. Phys. Chem. Solids* **135**, 109058 (2019). <https://doi.org/10.1016/j.jpcs.2019.06.006>
 55. M.H. Phan, S.C. Yu, Review of the magnetocaloric effect in manganite materials. *J. Magn. Magn. Mater.* **308**, 325–340 (2007). <https://doi.org/10.1016/j.jmmm.2006.07.025>
 56. V. Franco, A. Conde, D. Sidhaye, B.L.V. Prasad, P. Poddar, S. Srinath, M.H. Phan, H. Srikanth, Field dependence of the magnetocaloric effect in core-shell nanoparticles. *J. Appl. Phys.* **107**, 09A902 (2010). <https://doi.org/10.1063/1.3335514>
 57. H. Oesterreicher, F.T. Parker, Magnetic cooling near Curie temperatures above 300 K. *J. Appl. Phys.* **55**, 4334 (1984). <https://doi.org/10.1063/1.333046>
 58. V. Franco, A. Conde, J.M. Romero-Enrique, J.S. Blázquez, A universal curve for the magnetocaloric effect: an analysis based on scaling relations. *J. Phys.: Condens. Matter* **20**, 285207 (2008). <https://doi.org/10.1088/0953-8984/20/28/285207>
 59. V. Franco, J. Blázquez, A. Conde, Influence of Ge addition on the magnetocaloric effect of a Co-containing nanoperm-type alloy. *J. Appl. Phys.* **103**, 07B316 (7) (2008). <https://doi.org/10.1063/1.2835688>
 60. N.A. Liedienov, Z. Wei, V.M. Kalita, A.V. Pashchenko, Q. Li, I.V. Fesych, V.A. Turchenko, C. Hou, X. Wei, B. Liu, A.T. Kozakov, G.G. Levchenko, Spin-dependent magnetism and superparamagnetic contribution to the magnetocaloric effect of non-stoichiometric manganite nanoparticles. *Appl. Mater. Today* **26**, 101340 (2022). <https://doi.org/10.1016/j.apmt.2021.101340>
 61. V. Franco, J.S. Blázquez, A. Conde, Field dependence of the magnetocaloric effect in materials with a second order phase transition: a master curve for the magnetic entropy change. *Appl. Phys. Lett.* **89**, 222512 (2006). <https://doi.org/10.1063/1.2399361>

Springer Nature or its licensor (e.g. a society or other partner) holds exclusive rights to this article under a publishing agreement with the author(s) or other rightsholder(s); author self-archiving of the accepted manuscript version of this article is solely governed by the terms of such publishing agreement and applicable law.